PAPER • OPEN ACCESS

3D printed fiber sockets for plug and play micro-optics

View the article online for updates and enhancements.

3D printed fiber sockets for plug and play micro-optics

Parvathi S Nair[1] ⓘ **, Jonathan Trisno**[1]**, Hongtao Wang**[1] **and Joel K W Yang**[1,2]

[1] Singapore University of Technology and Design, 8 Somapah Road, 487372, Singapore
[2] Institute of Materials Research and Engineering (IMRE), A*STAR, 138634, Singapore

E-mail: joel_yang@sutd.edu.sg

CrossMark

Abstract

Integrating micro-optical components at the end facet of an optical fiber enables compact optics to shape the output beam (e.g. collimating, focusing, and coupling to free space elements or photonic integrated circuits). However, the scalability of this approach is a longstanding challenge as these components must be aligned onto individual fiber facets. In this paper, we propose a socket that enables easy slotting of fibers, self-alignment, and coupling onto micro-optical components. This integrated socket can be detached from the substrate upon fiber insertion to create a stand-alone optical system. Fabrication is done using nanoscale 3D printing via two-photon polymerization lithography onto glass substrates, which allows multiple sockets to be patterned in a single print. We investigated variations in socket design and evaluated the performance of optical elements for telecom wavelengths. We obtained an alignment accuracy of ∼3.5 μm. These socket designs can be customized for high efficiency chip to fiber coupling and extended to other spectral ranges for free-form optics.

Keywords: integrated socket, alignment, fiber slotting, fiber connector, two-photon polymerization lithography

(Some figures may appear in colour only in the online journal)

1. Introduction

Advancements in femtosecond laser two-photon polymerization lithography (TPL) offers unprecedented capabilities to produce customizable 3D prints down to submicron length scales. This lithographic technique has simplified many of the complex fabrication processes, enabling direct printing from a designer's digital model. Optical systems have been realized in the past using various fabrication techniques, examples of which include injection molding, inkjet printing with UV-curable hybrid polymer and direct laser writing techniques [1–8]. However, these methods have limited scope due to alignment limitations [1–3, 9] and design restrictions [10]. Femto-second laser pulses and two-photon absorption have simplified the fabrication process, enabling us to conveniently fabricate micro- and nanometer scale devices [11–17]. A variety of conventional and free-form lenses have been directly printed onto fiber tips using TPL [14, 16, 17]. These free-form optical elements find applications in fiber-based endoscopy [18, 19], tomography [20] and other imaging applications. However, this fabrication procedure requires customized fiber mounting setups, and *in-situ* alignment to individual optical fibers prior to printing. The method of selective polymerization to fabricate microtips to generate Bessel-like beams [21] enables beam shaping without alignment limitations. Though a promising approach, it will be difficult to apply this method to the fabrication of complex lenses and optical systems as the convex photopolymer droplet on the fiber tip limits the shape and size of the fabricated structures. Thus, approaches that enable scaling and rapid evaluation of multiple optical designs are vital.
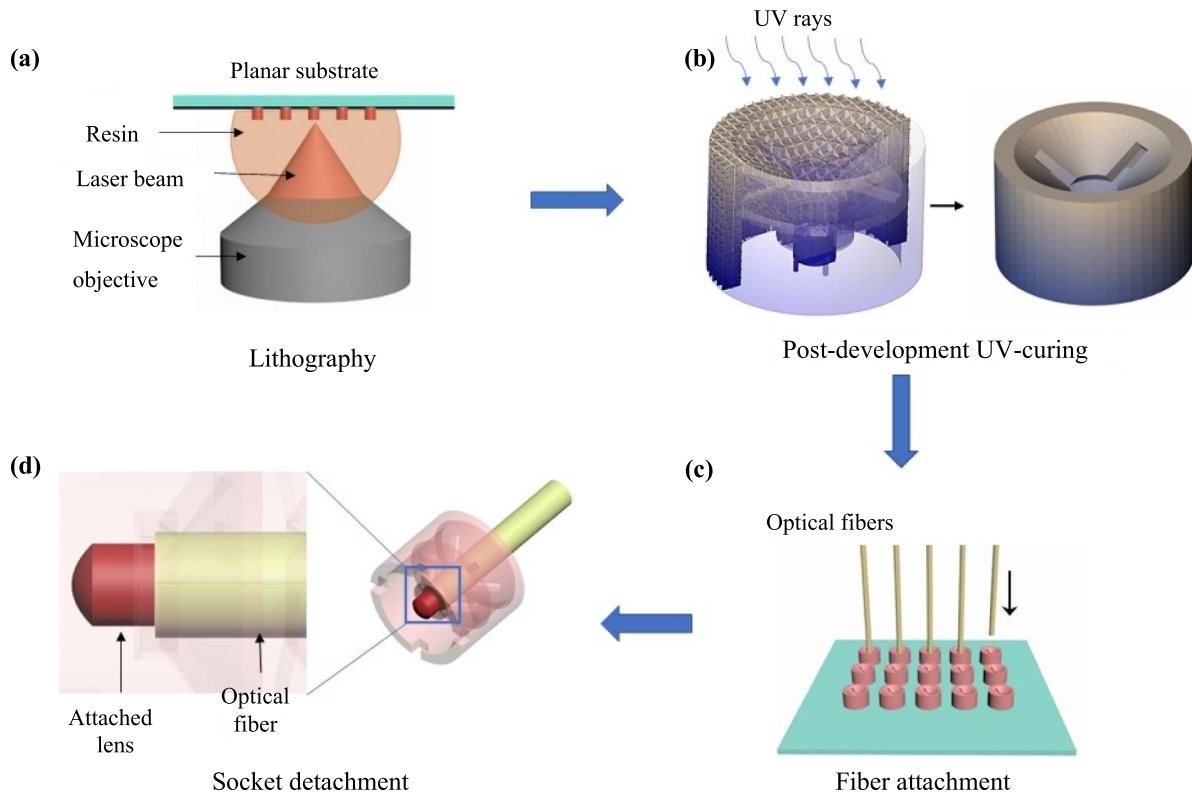
Figure 1. Process flow producing multiple detachable sockets at a time onto a handle substrate. (a) Lithographic patterning using a femtosecond laser TPL to crosslink the outer shell and scaffold of the design structures. (b) Post-development UV-curing to solidify internal resin. (c) Fiber attachment via manual insertion of fibers by eye or multiple fibers simultaneously through automation. (d) Socket detachment from handle substrate resulting in optical elements self-aligned at the end facet of fibers.

In this paper, we propose a fiber socket integrated with micro-optical components that are 3D printed using TPL. This socket is designed to (1) leverage on mature nanofabrication processes based on flat substrates, (2) eliminate the need for printing directly on the fiber facets, and (3) allow flexibility in designing and attaching arbitrary optical components using simpler alignment techniques. Without the aid of manipulators or magnifiers, cleaved bare fibers are manually slotted into the socket. The end facets come in contact with the optical components, and the entire 3D print is later detached from the handle substrate. This approach enables the prototyping of optical components because multiple sockets with different optical components can be printed in a single fabrication step. Based on the intended applications, the appropriate optical component is selected and attached to the fiber in a plug-and-play manner. Compared to direct fabrication on fiber facets, this method is scalable and allows for higher throughput production.

2. Design

2.1. Concept

The proposed method, as depicted in figure 1, enables bulk fabrication of optical components along with the insertion socket on flat substrates. During CAD modelling, the optical component is centred with the socket so that it can align with the fiber after attachment. Optical fibers can be inserted after the entire fabrication is done and both the integrated socket and its optical component can be detached from the substrate after fiber insertion. If there is a change in requirement, the component can be easily removed using a fiber cleaning wipe and a new component can be attached. Reusing the optical component will be difficult as the removal process damages the socket.

2.2. Design of fiber socket

The design considerations for the proposed socket were (1) gripping and holding strength to keep the fiber in position, (2) axial and lateral alignment to the micro-optical component fabricated on the socket tip, (3) ease of fiber insertion into the socket and detachment of socket from handle substrate. We used a double slot design (figure 2(a)), where two layers of conical fins align and guide the fiber as it is inserted perpendicular to the substrate. This design avoids potential tilting of the fiber that can cause optical losses due to off axis beam tilt. We use fibers with normally cleaved facets. The conical fins serve two purposes: (1) they taper inwards to guide the fiber into the socket base plate and (2) provide holding force that keeps the socket in place. The diameter of the circular opening at the bottom of the fins are 5% smaller than the diameter of the fiber. As a result, the fins flex outwards as the fiber is inserted. A support bar is introduced between the conical guiding
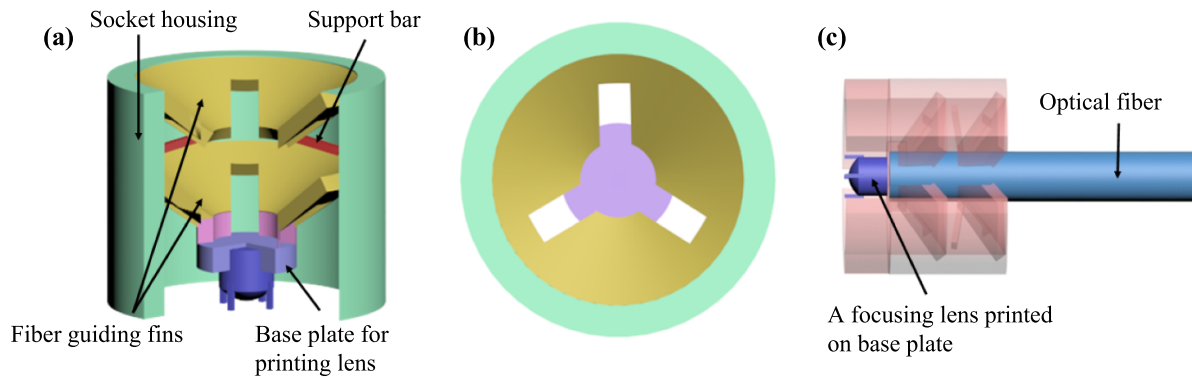
Figure 2. (a) Schematic of the fiber socket design. (b) Top view. (c) Schematic of the socket integrated with a lens and attached to an optical fiber.

fins and the socket housing to apply holding forces that press the fins onto the fiber. The base plate acts as a physical barrier for the end facet of the fiber to butt up against. This plate also provides a strong grip for the optical component and prevents it from dislodging during fiber insertion. The thickness of the base plate determines the separation distance between the fiber facet and the micro-optical components, thus allowing for precise axial positioning (figure 2(c)). Optical component design should consider potential beam divergence due to the base plate. This divergence can be calculated from the thickness of the plate and the refractive index of the material used for fabrication. The fabricated device is easy to insert and remove, making it convenient for testing and prototyping. Alternatively, UV curable epoxy can be used to permanently attach the fiber and avoid unintentional detachment.

3. Fabrication and testing

The structures were fabricated using TPL with a commercial femtosecond laser lithography system, Photonic Professional GT, from Nanoscribe GmbH. The socket design was modelled in 3ds Max. The standard tessellation language file generated was converted to a Nanoscribe general writing language (GWL) file using DeScribe, the slicing and hatching tool from Nanoscribe. The slicing and hatching parameters were set based on the optimal printing time and the structure's rigidity. Contrary to conventional 3D printing, in TPL, polymerization happens within the puddle of resin and the structure is embedded in the resin until the development process. In this technique, polymerization is quite fast, which makes overhangs and unsupported structures less of a concern compared to fused deposition modelling printing. Nevertheless, the optical component anchored to the handle substrate is printed first and the socket is printed next. This sequencing allows the optical component to serve as a supporting base to grow the bottom guiding fin. The support bars attached to the socket housing (figure 2(a)) act as an anchor point for the upper guiding fin during the polymerization.

The socket was fabricated in Nanoscribe's IP-S resist, which is a proprietary negative-tone resist compatible with the $25\times$ magnification, 0.8 numerical aperture (NA) objective

lens. IP-S has lower shrinkage and higher mechanical stability [22, 23] compared to other IP-series resists. IP-S produces smoother surfaces upon fabrication, making it the preferred resist for this fiber socket. It also exhibits high optical qualities (transmittance > 95%) making it a good choice for fabricating optical components [19]. These factors facilitate the entire fabrication process to be done in a single step.

Fabrication was done on an indium tin oxide (ITO)-coated glass substrate. The ITO-coated glass substrate has a refractive index that contrasts with the photoresist, which makes the interface between the resist and substrate easily identifiable during printing. The estimated printing durations obtained from Nanoscribe's DeScribe software suggested that fabrication with IP-S would be 35 times faster than the structures written with IP-Dip, which is another IP-series resist commonly used for fabricating optical components. To further speed up the printing process, the socket structure was fabricated using the 'shell-and-scaffold' writing pattern. Shell and scaffold writing reduced printing time by ~80% compared to solid writing. This writing strategy patterns only the outer surfaces (shell) of the 3D geometry and some internal infill structures (scaffold) that hold the shell together. Therefore, it poses a risk of resist leakage, especially in cases where the voxel tip is positioned at the substrate-resist interface. To ensure a 'resist-tight' structure, the interface position was set to 0.8 μm inside the substrate based on the slicing distance in the GWL file before fabrication.

During sample development, uncured resist was removed from outside the shell by immersing the sample in polyethylene glycol methyl ether acetate (PGMEA—30 min), isopropyl alcohol (IPA—5 min), and nonafluorobutyl methyl ether (NFBME—5 min) [24]. Finally, post-development UV exposure was performed to cure the resist inside the shell and enhance the overall strength of the structure.

The final structures were detached from the handle wafer by applying localized stress at the base of the print. Other conventional methods for detaching a printed structure include printing small support posts upon which the entire structure rests [25], loosening the structure with a wire or fiber mounted on a micromanipulator [26], or using sacrificial layers that can be dissolved and loosening the structure with a razor blade [27]. We observed that the structures adhered well to the handle
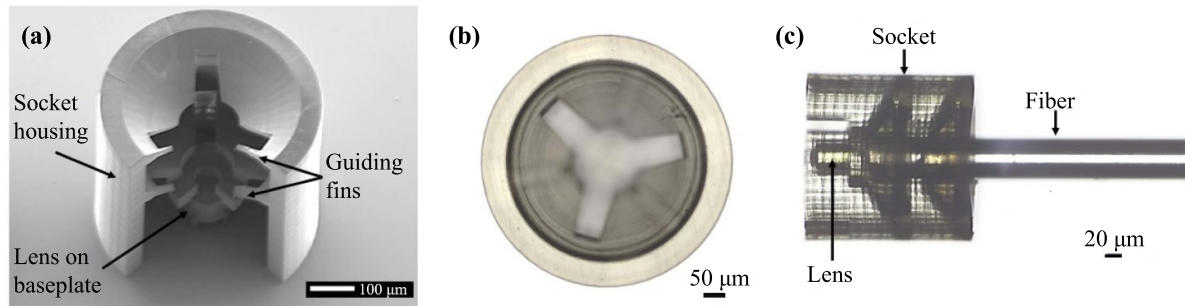
Figure 3. (a) SEM image of the fiber holder with the focusing lens attached to the base plate. (b) Optical micrograph of the integrated socket (top view). (c) Optical micrograph of a fiber inserted into the fabricated socket (side view).
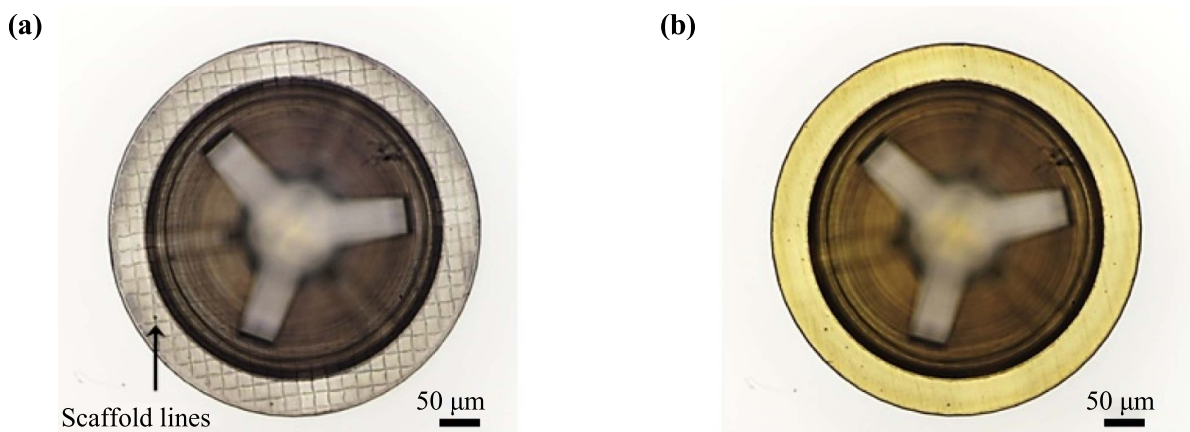

Figure 4. Optical micrographs of socket structure before and after UV curing.

wafer as the fiber was slotted in, despite some inevitable lateral forces imparted during the manual process. However, once the fiber was inserted, the structure could be readily detached either by sliding a razor blade or pushing sharp tweezers at the base.

Figure 3(a) shows the SEM image of the fiber socket with a focusing lens printed on the base plate. This structure was fabricated with a cut-out section that left the guiding fins, base plate, and the lens exposed for SEM inspection. The lens was elevated from the base with the help of support legs, so its surface remained intact during the socket detachment process. Figures 3(b) and (c) show optical microscope images of the fabricated fiber socket structure before and after fibre insertion. A single mode fiber from Thorlabs (part number 1550BHP) with a cladding diameter of 125 ± 1.0 μm, was manually inserted into the socket without the aid of a microscope. The dual acrylate coating layer was carefully stripped off from the fiber end before insertion.

The lens and socket in figure 3(c) were fabricated using the same photoresist (IP-S), making the entire fabrication a single-step process. However, the lens was fabricated as a solid object with uniform exposure throughout the structure while the socket was fabricated as a shell with internal support scaffolds for optimal writing speed. The lines visible on the socket structure (figure 3(c)) are due to the 'floor planes' (horizontal layers separating the infills) which were 20 μm apart. These

floor planes contributed to the stability of the scaffold and prevented the shell from bulging. Optical components were fabricated at a slicing distance of 300 nm, rendering smooth surfaces and hence minimal optical scattering. The socket structures lacked the strength to withstand fiber insertion and the guiding fins were damaged in the insertion process. Therefore, the socket-lens assembly was UV cured (TechnoDigm UVF400/600 UV curing system, with 350 mW cm^{-2} UVA intensity) for 15–20 min to crosslink the unpolymerized resist inside the shell and improve mechanical stability [22].

Figure 4 shows the optical micrograph of the socket structure before and after curing. The structure developed a yellow color during UV curing [28], as seen in figure 4(b). The scaffold lines are clearly visible in figure 4(a) as the resist had a higher refractive index once it was polymerised [23]. The absence of scaffold lines in figure 4(b) shows that the unpolymerized resin between the scaffolds polymerizes under UV exposure and the entire structure solidifies. As previously reported [29], the refractive index of a two-photon polymerized resist is lower than its UV-exposed bulk counterpart (Δn up to 0.01). However, UV exposure of two-photon polymerized layers does not cause further curing or affects its refractive index. Hence, UV curing the entire structure to increase the strength of the socket does not cause any unintended deviation in the lens behavior.
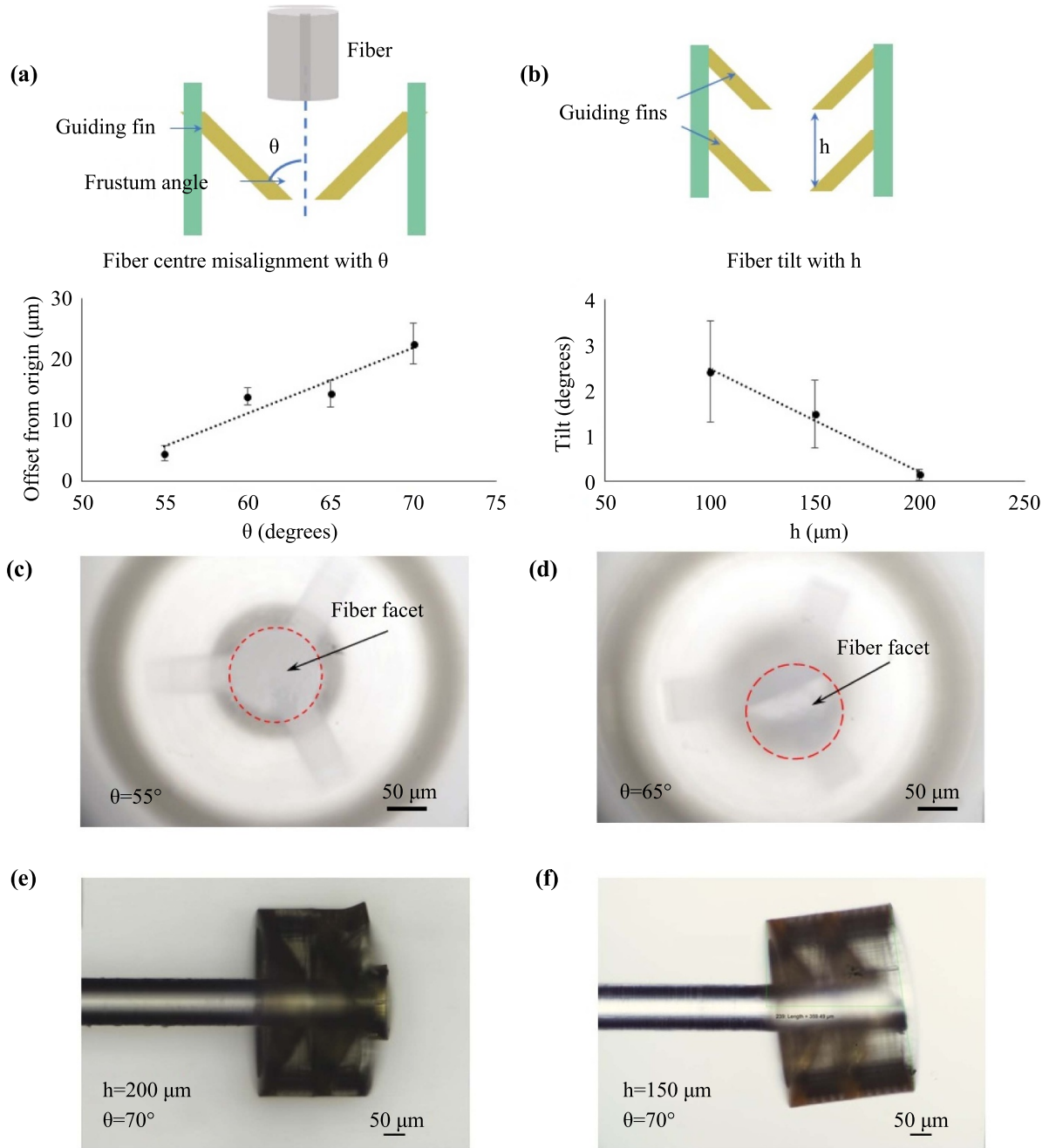
Figure 5. Fiber lateral and tilt alignment dependence on frustrum angle and separation of guiding fins. (a) Plot of lateral misalignment vs. frustum angle, for $h = 200\ \mu$m. Measurements for $55°$ is closer to the origin, indicating maximum alignment. (b) Fiber tilt measured as a function of spacing (h) between guiding fins, keeping frustum angle $= 55°$. Tilt measurements are done for spacings of $100\ \mu$m, $150\ \mu$m, and $200\ \mu$m. (c) Optical micrograph of a fiber (marked in red) aligned with the socket base as imaged from the bottom. (d) A mis-aligned fiber. (e) Side image showing fiber inserted without tilt. (f) Fiber tilted due to lower h value.

4. Results and discussion

The effectiveness of the socket in holding the fiber and aligning it with the optical component on the base plate was characterised. Of the multiple design parameters that affect fiber insertion and positioning, two were chosen for analysis: (1) frustum angle, θ and (2) spacing between guiding fins, *h*.

Alignment offset was measured by calculating the offset between the centres of the socket and fiber facet. This offset was measured as a function of frustum angle, which is

defined as the angle between the fiber axis and the guiding fins. Four different frustum angles ($55°$, $60°$, $65°$, $70°$) were tested with ten samples each (figure 5(a)). It was observed that for higher frustum angles ($70°$), the guiding fins were susceptible to damage during fiber insertion, which compromised the alignment. For frustum angles above $70°$, the guiding fins were severely damaged, causing the socket to fall off the fiber tip. At a lower frustum angle ($55°$), the guiding fins withstood the deflections during insertion. Such structures effectively guide the fiber to the base and hold it in position. Figures 5(c) and (d)
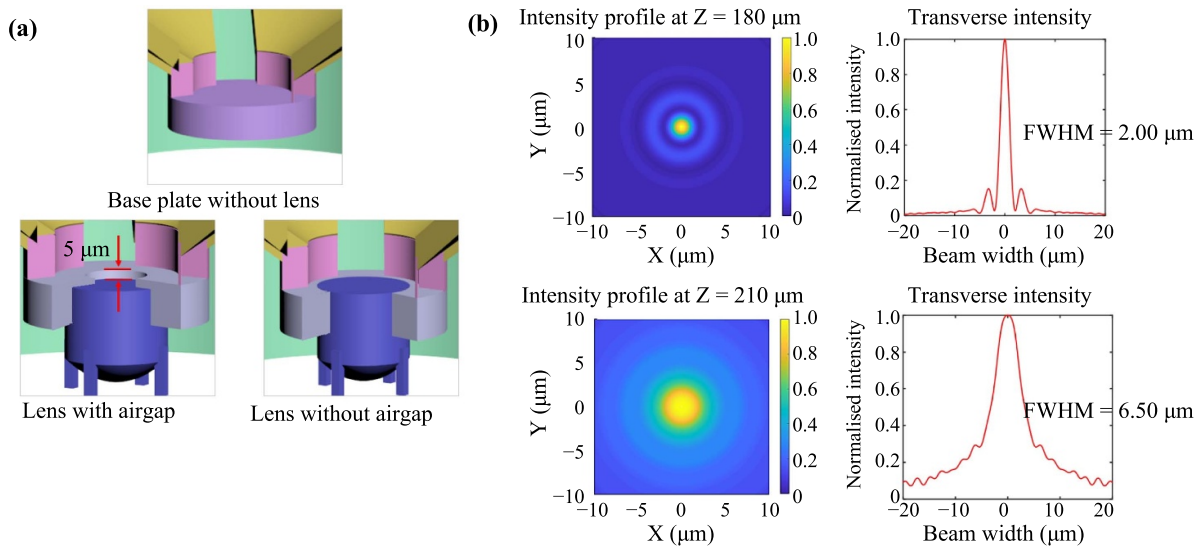
Figure 6. (a) Schematic of lens configurations tested. (b) Simulation results at focal point ($Z = 180$ μm) and measured distance ($Z = 210$ μm).

show the optical micrographs comparing an aligned and a misaligned fiber. For $\theta = 55°$, average accuracy was ~4.5 μm and the best possible alignment measured had a centre offset of 3.56 μm. The highest offset measured for $\theta = 70°$ was 26.39 μm. Highest yield estimated was between 83% and 91% for socket structures with $\theta = 55°$ and h fixed at 200 μm.

As tilting of fiber was a concern, it was tested for different spacing between the guiding fins (h). Spacing (h) is defined as the base-to-base distance between the top and bottom guiding fins. Figure 5(b) shows the tilt measurements conducted for three different h values (100 μm, 150 μm, 200 μm). A set of five holders were tested in each case to ensure repeatability. Figures 5(e) and (f) show sample images of non-tilted and tilted fibers. For a separation of 100 μm, an average tilt of ~2.4° was observed. The tilt was minimal (~0.02°) when the separation between the conical guiding fins was 200 μm. This separation was used in subsequent experiments, as increasing the separation beyond 200 μm would impose restrictions on the thickness of the optical component fabricated to maintain the overall structure height, which was capped at 500 μm. The number of guiding fins were limited to two in both the tests as it is the minimum number of fins required to align and hold the fiber inserted perpendicular to the base. Increasing the number of guiding fins can improve the accuracy and hold the fiber more effectively. But this increase may increase the fabrication time.

To investigate losses due to reflections at the end facet, coupling with a base plate and focusing lens on the base plate of the socket were performed with three configurations, as shown in figure 6(a). The first configuration (top) only includes the base plate, without a lens. The bottom configurations show the lens separated from the fiber facet with a 5 μm airgap and the lens in contact with the fiber facet. The lens in both the configurations was designed to focus the incoming beam at 180 μm with the spot size of ~5.17 μm. The power measurements over a wavelength range of 1.50 μm to 1.63 μm

showed a maximum transmittance at 1.6 μm. The output from the configurations in figure 6(a) was measured with a beam analyzer (Duma optronics Ltd with a BA-3 InGaAs detector head).

The 2D projection and the profile along the V axis—which was 45° from the base of detector head—measured for 1.6 μm wavelength are shown in figure 7. A schematic of the measurement configuration is shown in the inset. The profiles obtained from the beam analyzer software include a measured graph as well as its gaussian fit (GF). The GF in this case is defined as a least-squares fit of a gaussian equation to the cross-section beam profiles. This profile is automatically calculated by the software during the measurement using the relation: $I = Ve^{[-(x-c)/\sigma]^2}$, where I is the intensity of a pixel at location x. The peak intensity of the GF curve (V), centroid of the GF peak (C), and the diameter of the GF curve at the 13.5% intensity level (Mode Field Diameter (MFD), σ) were derived by performing a least-squares fit on this equation. Intensity profiles simulated for the lens at two longitudinal positions: $Z = 180$ μm (focal point) and $Z = 210$ μm are shown in figure 6(b).

As the beam analyzer detector has multiple scanning knife-edges on a rotating drum, measurements can only be taken at a minimum distance from the fiber tip. This distance was calculated as 175.42 μm from the reference measurements. With this minimum distance and the position of the lens on the socket, the measuring point after lens attachment was approximately 210 μm away from the lens facet. Figure 7(a) shows the reference measurements, which were taken from a bare fiber. The fiber was placed at the closest possible position to the beam analyzer sensor. A circular beam profile with a full width half maximum (FWHM) of 25.88 μm was obtained at this position. Figure 7(b) shows the beam profile for the case of a socket with the 5 μm thick base plate alone. The resulting beam had a circular profile with an increased FWHM of 35.23 μm and a transmittance efficiency of 93.74%. The
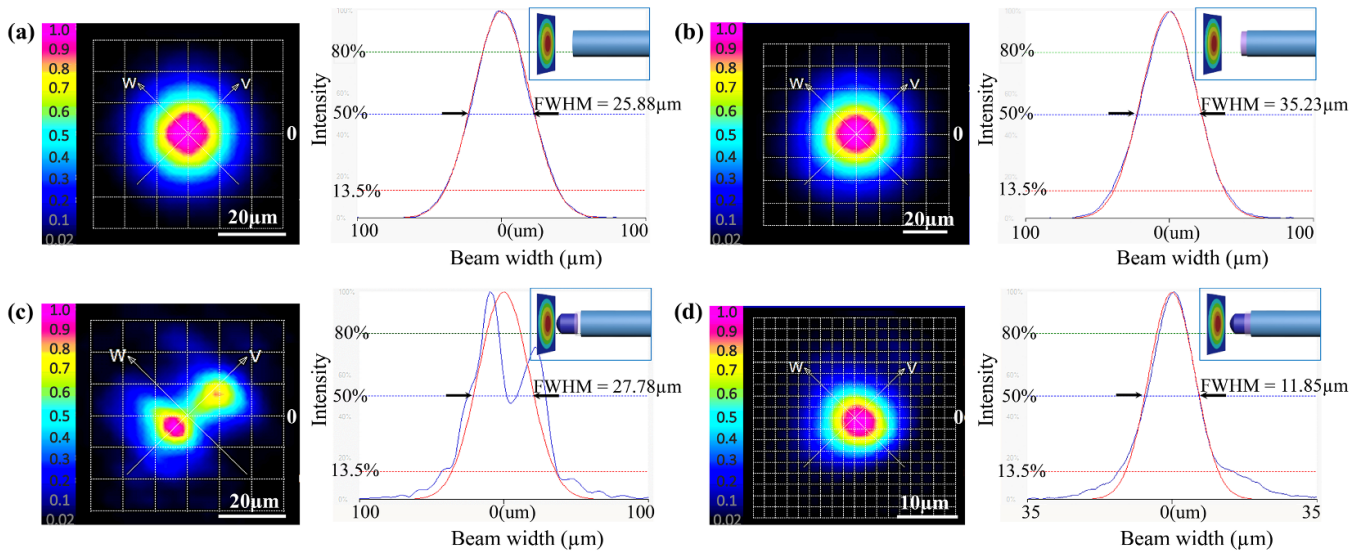
Figure 7. Beam profile measurements. (a) Beam from a bare fiber (schematic of measuring configuration inset). (b) Output from a 5 μm base plate without a lens. (c) Output from lens attachment with airgap. (d) Output from lens attachment without airgap, (c) and (d) were measured at a Z position of ~210 μm. The blue curve in the graph shows the measured profile and the red curve shows the corresponding gaussian fit.

lens-socket configurations in figure 6(a) were tested with these references as input.

The configuration with 5 μm airgap delivered a distorted output with multiple peaks, as presented in figure 7(c). Although the second peak did not have 100% intensity, the profile was prominent along the V axis, which contributed to the increased beam width. The elliptical major and minor axes measured 52.92 μm and 35.66 μm respectively with an orientation of 75°. Thus, the output spot size was larger compared to the spot size from a bare fiber and was no longer circular. The transmittance efficiency for this configuration was 66.5% based on the power measurements. For the configuration without airgap, the FWHM was 11.85 μm (figure 7(d)). The major and minor beam profiles had an average difference of only 2.75 μm, which can be approximated as a circular beam. The power measurements obtained from the beam analyzer revealed a transmittance efficiency of 69.35%. The clip levels for measurements were set to 13.5% (MFD), 50% (FWHM), and 80%. The configuration without airgap and proper attachment showed superior performance in terms of focusing and transmittance efficiency. The mismatch between the FWHM simulated value (~7 μm) and the experimental value (~12 μm) can be attributed to the practical difficulty of manually adjusting the measurement position and minor vibrations of the fiber during measurement or fabrication imperfections of the optical component. The measured value for bare fiber and the lens attached without airgap had higher correlation with the corresponding GF. For lens attachment with airgap, GF and measured values had a prominent deviation along the V-axis, with a maximum difference of 10.02 μm.

5. Conclusion

We designed and 3D printed fiber sockets integrated with a lens (or generally any micro-optical elements) that can be used as an alternative to direct fabrication on fiber facets. This socket design tackles the alignment challenges between the fiber and the optical elements and increases the throughput for applications involving modification and processing of beams from an optical fiber. Optical fibers can be manually inserted into these sockets without the aid of complex alignment micromanipulators. Detaching the socket from the flat handling substrate enables the fiber-socket-optical component to be a stand-alone system that can be independently placed anywhere in a test setup. The 'all 3D printed' nature of the process opens opportunities to customize any optical element at the end of the socket design. The initial lens design used in this paper exhibited a transmission efficiency of ~70% with the possibility for further improvements. The on-axis alignment accuracy for the socket was ~3.5 μm with a tilt alignment of ~0.02°. Compared to existing designs of alignment-tolerant optical devices, our fabrication method allows optical components to be rapidly 3D printed—due to the mostly hollow design—and to be detached from the substrate upon fiber insertion, enabling rapid prototyping of standalone optical systems.

ORCID iD

Parvathi S Nair ⬚ https://orcid.org/0000-0003-3095-9872

References

[1] Popovic Z D, Sprague R A and Connell G A N 1988 Technique for monolithic fabrication of microlens arrays *Appl. Opt.* **27** 1281–4

[2] Lee S K, Lee K C and Lee S S 2002 A simple method for microlens fabrication by the modified LIGA process *J. Micromech. Microeng.* **12** 334–40

[3] Lee B K, Kim D S and Kwon T H 2004 Replication of microlens arrays by injection molding *Microsyst. Technol.* **10** 531–5

[4] Kim J Y, Brauer N B, Fakhfouri V, Boiko D L, Charbon E, Grutzner G and Brugger J 2011 Hybrid polymer microlens arrays with high numerical apertures fabricated using simple ink-jet printing technique *Opt. Mater. Express* **1** 259–69

[5] Völkel R, Eisner M and Weible K J 2003 Miniaturized imaging systems *Microelectron. Eng.* **67–68** 461–72

[6] Kuang D F, Zhang X L, Gui M and Fang Z L 2009 Hexagonal microlens array fabricated by direct laser writing and inductively coupled plasma etching on organic light emitting devices to enhance the outcoupling efficiency *Appl. Opt.* **48** 974–8

[7] Yang R, Wang W J and Soper S A 2005 Out-of-plane microlens array fabricated using ultraviolet lithography *Appl. Phys. Lett.* **86** 161110

[8] Hoy C L, Durr N J, Chen P Y, Piyawattanametha W, Ra H, Solgaard O and Ben-Yakar A 2008 *Opt. Express* **16** 9996–10005

[9] Biehl S, Danzebrink R, Oliveira P and Aegerter M A 1998 Refractive microlens fabrication by ink-jet process *J. Sol-Gel Sci. Technol.* **13** 177–82

[10] Brückner A, Oberdörster A, Dunkel J, Reimann A, Müller M and Wippermann F 2014 Ultra-thin wafer-level camera with 720p resolution using micro-optics *Proc.* SPIE *9193 Novel Optical Systems Design and Optimization XVII* 91930W (San Diego, California, United States: SPIE)

[11] Zappe H P 2010 *Fundamentals of Micro-optics* (Cambridge: Cambridge University Press)

[12] Malinauskas M, Gilbergs H, Žukauskas A, Purlys V, Paipulas D and Gadonas R 2010 A femtosecond laser-induced two-photon photopolymerization technique for structuring microlenses *J. Opt.* **12** 035204

[13] Malinauskas M *et al* 2010 Femtosecond laser polymerization of hybrid/integrated micro-optical elements and their characterization *J. Opt.* **12** 124010

[14] Williams H E, Freppon D J, Kuebler S M, Rumpf R C and Melino M A 2011 Fabrication of three-dimensional micro-photonic structures on the tip of optical fibers using SU-8 *Opt. Express* **19** 22910–22

[15] Malinauskas M, Farsari M, Piskarskas A and Juodkazis S 2013 Ultrafast laser nanostructuring of photopolymers: a decade of advances *Phys. Rep.* **533** 1–31

[16] Gissibl T, Schmid M and Giessen H 2016 Spatial beam intensity shaping using phase masks on single-mode optical fibers fabricated by femtosecond direct laser writing *Optica* **3** 448–51

[17] Gissibl T, Thiele S, Herkommer A and Giessen H 2016 Sub-micrometre accurate free-form optics by three-dimensional printing on single-mode fibres *Nat. Commun.* **7** 11763

[18] Coquoz O, Conde R, Taleblou F and Depeursinge C 1995 Performances of endoscopic holography with a multicore optical fiber *Appl. Opt.* **34** 7186–93

[19] Gissibl T, Thiele S, Herkommer A and Giessen H 2016 Two-photon direct laser writing of ultracompact multi-lens objectives *Nat. Photonics* **10** 554–60

[20] Li J W *et al* 2018 Two-photon polymerisation 3D printed freeform micro-optics for optical coherence tomography fibre probes *Sci. Rep.* **8** 14789

[21] Tan J Y, Yu R W and Xiao L M 2019 Bessel-like beams generated via fiber-based polymer microtips *Opt. Lett.* **44** 1007–10

[22] Liu Y, Stein O, Campbell J H, Jiang L J, Petta N and Lu Y F 2017 Three-dimensional printing and deformation behavior of low-density target structures by two-photon polymerization *Proc. SPIE 10354 Nanoengineering: Fabrication, Properties, Optics, and Devices XIV* 103541U (San Diego, CA: SPIE)

[23] Liu Y, Campbell J H, Stein O, Jiang L J, Hund J and Lu Y F 2018 Deformation behavior of foam laser targets fabricated by two-photon polymerization *Nanomaterials* **8** 498

[24] Sample development (available at https://support.nanoscribe.com/hc/en-gb/articles/360001344673)

[25] Radke A, Gissibl T, Klotzbücher T, Braun P V and Giessen H 2011 Three-dimensional bichiral plasmonic crystals fabricated by direct laser writing and electroless silver plating *Adv. Mater.* **23** 3018–21

[26] Phillips D B, Padgett M J, Hanna S, Ho Y L D, Carberry D M, Miles M J and Simpson S H 2014 Shape-induced force fields in optical trapping *Nat. Photonics* **8** 400–5

[27] Removal and stripping (available at: https://support.nanoscribe.com/hc/en-gb/articles/360002773914)

[28] Curing printed structures (available at: https://support.nanoscribe.com/hc/en-gb/articles/360002022373)

[29] Dottermusch S, Busko D, Langenhorst M, Paetzold U W and Richards B S 2019 Exposure-dependent refractive index of nanoscribe IP-Dip photoresist layers *Opt. Lett.* **44** 29–32